Femtosecond pump-probe near-field optical microscopy

B. A. Nechay,[a] U. Siegner, M. Achermann, H. Bielefeldt,[b] and U. Keller
Swiss Federal Institute of Technology Zurich, Institute of Quantum Electronics, ETH Hönggerberg-HPT, CH-8093 Zürich, Switzerland

(Received 8 December 1998; accepted for publication 2 March 1999)

We have developed an instrument for optically measuring carrier dynamics in thin-film materials with ~150 nm lateral resolution, ~250 fs temporal resolution, and high sensitivity. This is achieved by combining ultrafast pump-probe laser spectroscopic techniques, which measure carrier dynamics with femtosecond-scale temporal resolution, with the nanometer-scale lateral resolution of near-field scanning optical microscopes (NSOMs). We employ a configuration in which carriers are excited by a far-field pump laser pulse and locally measured by a probe pulse sent through a NSOM tip and transmitted through the sample in the near field. A novel detection system allows for either two-color or degenerate pump and probe photon energies, permitting greater measurement flexibility over earlier published work. The capabilities of this instrument are proven through near-field degenerate pump-probe studies of carrier dynamics in GaAs/AlGaAs single quantum well samples locally patterned by focused-ion-beam (FIB) implantation. We find that lateral carrier diffusion across the nanometer-scale FIB pattern plays a significant role in the decay time of the excited carriers within ~1 μm of the implanted stripes, an effect which could not have been resolved with a far-field system. © *1999 American Institute of Physics.* [S0034-6748(99)03106-8]

I. INTRODUCTION

Many dynamical processes in condensed matter and molecular or atomic systems take place on picosecond or subpicosecond time scales. Examples include energy relaxation in semiconductor systems[1] and charge transfer processes in molecular nanostructures.[2] Though a variety of measurement techniques can probe such dynamical processes, only all-optical techniques have reliably achieved subpicosecond temporal resolution. Ultrafast optical spectroscopic techniques have yielded a wealth of information about dynamics of electronic excitations in a variety of materials.[1,2] However, the diffraction limited lateral resolution of conventional far-field techniques limits the physical information which can be obtained about the properties of nanometer-scale lateral structures, since their inherent inhomogeneity cannot be spatially resolved. Furthermore, far-field measurements can tell us little about the transport mechanisms on the submicron lateral scale. The investigation of ultrafast dynamical processes on the nanometer scale has gained increasing interest in recent years with improvements in nanofabrication technologies leading to nanostructures with potential applications in fields such as lasers and electronic devices.[3] Therefore, combining ultrafast all-optical spectroscopic techniques with the advantages of high spatial resolution in an instrument that measures optical signals in the near field would prove invaluable in exploring such processes. Although alternate means of measuring near-field optical signals exist,[4] near-field scanning optical microscopy (NSOM),[5,6] in which a nanometer-scale aperture at the end of a fiber is scanned in the near field of a sample, is the most established and easiest to interpret. NSOM has proven useful in exploring nanometer-scale physics and chemistry in a variety of materials.[4] Recently, a number of groups have successfully combined NSOM with ultrafast optical spectroscopic techniques to measure carrier dynamics with femtosecond-scale temporal resolution and nanometer-scale lateral resolution.[7–10] This article presents the development of a new instrument of this class, which combines a femtosecond pump-probe technique with NSOM, and discusses the issues involved. A novel detection system design adds measurement flexibility by allowing for both degenerate and two-color measurements. Ultrafast measurements of carrier dynamics in nanometer-scale ion implanted single quantum well samples demonstrate the capabilities of the system—~150 nm spatial resolution, ~250 fs time resolution, and high sensitivity—and show that information about physical processes can be obtained that is not accessible with far-field systems.

II. BACKGROUND

In pump-probe experiments, a pump pulse excites carriers in the sample. These excited carriers modify the absorption and the refractive index probed by a subsequent probe pulse. The measurement of the differential probe transmission signal, i.e., $\Delta T * P_{\text{probe}} * \eta$, or reflection signal, i.e., $\Delta R * P_{\text{probe}} * \eta$, versus pump-probe time delay gives a measure of the dynamics of the excited carrier population. Here, $\Delta T = T_{\text{pump on}} - T$ and $\Delta R = R_{\text{pump on}} - R$ (i.e., the pump-induced changes in the probe), T and R are the linear transmission and reflection of the probe, respectively, P_{probe} is the probe power incident on the sample, and η is the collection

[a]Electronic mail: nechay@iqe.phys.ethz.ch
[b]Present address: Experimentalphysik VI, Universitaet Augsburg, D-86135 Augsburg, Germany.

efficiency of the detection system. In the simplest case, ΔT and ΔR are proportional to the excited carrier concentration.[1]

The time resolution of such a measurement is limited only by the pump and probe pulsewidths. In all but a small handful of experiments, pump and probe excitations are done in the far field—limiting the achievable lateral resolution to the diffraction limit of $\lambda/2$. However, this limitation can be circumvented by incorporating the lateral resolution of NSOM.

In NSOM, a NSOM probe tip confines light to subwavelength dimensions by a nanometer-scale aperture at its apex. By raster scanning the tip across the sample in the near field, i.e., at tip-sample distances much less than the wavelength, nanometer-scale spatial variations of optical properties of the sample can be observed. The NSOM probe tip typically consists of an optical fiber which has been tapered to nanometer-scale dimensions through either pulling[6] or etching[11] techniques and then aluminum coated at 90° angles, forming a small, typically ~100 nm size aperture. This aperture size, along with the tip-sample flying height and thickness of the active region of the sample, determines the lateral resolution of NSOM.

One can envision various configurations combining femtosecond pump-probe techniques with NSOM. First, the pump and probe pulses can excite the sample either globally (i.e., far field) or locally (i.e., through the NSOM tip), allowing for three possibilities: global pump/local probe, local pump/global probe, and local pump and probe. Second, the probe signal can be measured either in reflection or transmission. Last, the excitation and detection can either be at two different wavelengths (i.e., two color) or they can be degenerate.

A few of these configurations have been realized by various groups. Stark *et al.*[7] used a two-color global pump/local transmitted probe configuration, where spectral filtering was used to avoid the detection of background pump light. Smith *et al.*[8] used a degenerate equal-pulse correlation setup[12] with both pump and probe sent through the NSOM tip. Vertikov *et al.*[10] used a global pump with the reflected probe measured in near-field collection mode, and used a two-color configuration to separate the differential reflection signal from the background pump light. Last, though not a pump-probe experiment according to the definition used in this article, Levy *et al.*[9] measured luminescence intensity autocorrelation using two equal power global pump pulses and picking up the luminescence with the NSOM tip. In this experiment, the higher pump photon energy was spectrally filtered out from the luminescence. In the system described in this article, a global pump/local transmitted probe configuration was chosen, shown in Fig. 1(a), with a novel detection system that allows for both degenerate or two-color excitation. This novel combination allows for a higher degree of measurement flexibility than earlier published work.[7–10]

The choice between global or local pump excitation is largely determined by the requirements of the chosen experiment. Global pump excitation was chosen mainly due to the greater excitation intensity that can be applied in the far field, as opposed to the near field. Specifically, pump excitation through the NSOM tip is limited in the maximum excitation intensity due to the very low power throughput of NSOM tips and the tip damage threshold of a few mW of input power to the fiber.[13,14] In global pump excitation, the excitation intensity is only limited by the damage thresholds of the sample so potentially larger nonlinear responses can be measured.

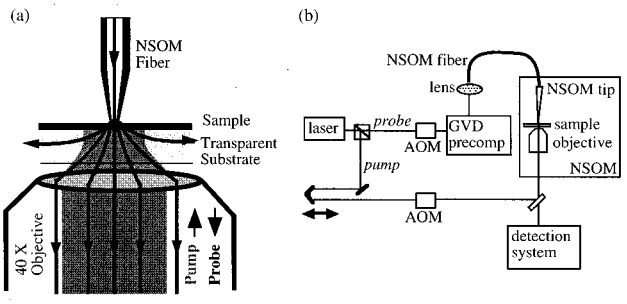

FIG. 1. (a) Global-pump, local-probe configuration, (b) experimental setup. AOM: acousto-optic modulator, GVD: group velocity dispersion.

Since global pump excitation was chosen, the differential probe transmission signal had to be measured locally with the NSOM tip. The main consideration in the decision between measuring in illumination versus collection mode was signal-to-noise. The general experience in the NSOM experiment community is that there is considerably more signal to work within illumination mode NSOM, as opposed to collection mode.[4] Therefore, the higher efficiency of illumination mode NSOM determined our preference for this configuration.

Signal-to-noise was also the main consideration in choosing a transmission geometry over a reflection geometry. Specifically, for samples which have comparable total reflected and transmitted powers, one would expect that a larger power can be measured in transmission than in reflection mode due to a larger solid angle of the collection optics in transmission. As for two-color versus degenerate experiments, the measurements discussed in this article were all done with degenerate pump probe, which suited the physics being explored for these samples.

III. EXPERIMENTAL SETUP

The experimental setup is shown in Fig. 1(b). The home-built NSOM instrument consists of either a pulled or etched NSOM tip whose aperture is held within ~10 nm of the sample surface using shear-force feedback.[15] Piezoelectric tuning fork shear force detection[16] is used to avoid the effects of scattered light which can be present in optical feedback techniques. In our case, we use a 32 768 Hz quartz tuning fork from Grieder Bauteile AG. The sample stage design and coarse and fine tip approach systems are similar to the designs described in Ref. 4, Secs. 5.3.4 and 5.5, respectively, while the coarse sample positioning is done with a manual translation stage. Both the feedback-controlled tip-sample flying height and the sample scanning are controlled by commercial Park Scientific Instruments Scanning Force Microscope electronics, which was adapted for the NSOM.

A mode-locked laser source (either a home-built Ti:sapphire or commercial Cr:LiSAF laser) generates a train of

~100 fs pulses, at a wavelength of ~840 nm and repetition rate of ~100 MHz, which is split into pump and probe pulses by a polarizing beamsplitter cube. The pump beam is sent through a motorized variable delay stage, which determines the time delay between the pump and probe pulses. It is then square-wave modulated at 1 MHz by an acousto-optic modulator (AOM) before being sent up through the NSOM objective and focused onto the sample. The probe pulse is first square-wave modulated at 1.05 MHz by an AOM and then sent through a group velocity dispersion (GVD) precompensation setup. The resulting negatively chirped probe pulse is then coupled into a single mode NSOM fiber, emerging at the output NSOM tip aperture with pulse widths typically below ~200 fs. The output from the NSOM tip aperture is transmitted through the thin sample in the near field and collected in the far field through the NSOM objective to the detection optics and avalanche photodiode (APD). Finally, the differential probe transmission signal is measured at the 50 kHz difference frequency using a lock-in amplifier. Last, the probe and back-reflected pump light collected by the NSOM objective lens can alternatively be directed to a charge-coupled device (CCD) imaging system to facilitate alignment for pump-probe spatial overlap.

IV. ISSUES OF CONCERN IN ULTRAFAST NSOM

In combining pump-probe spectroscopy with NSOM, various unique issues need to be considered. The most significant of these involve signal-to-noise considerations. Specifically, all NSOM systems are limited by the lack of high power throughput for apertures much smaller than the wavelength. For example, the most commonly used NSOM tips, also used in this experiment, are pulled or etched single-mode fibers whose power throughputs, for a 100 nm aperture at ~800 nm wavelengths, are typically $10^{-6}-10^{-4}$ for pulled tips and $10^{-5}-10^{-3}$ for etched tips. The throughput for etched tips is generally larger due to a larger cone angle, which minimizes the distance over which evanescent modes near the tip aperture must propagate, thereby minimizing the power loss. For both types of tips, the power throughput strongly depends on the aperture diameter, as d^6 from the Bethe model,[17] so that better spatial resolution comes at a great cost of useable signal power. Furthermore, since the maximum input power is limited to a few mW by the damage threshold of the aluminum fiber coating,[13,14] the resulting NSOM fiber output for a 100 nm aperture is typically less than 100 nW. In the case of pump-probe measurements, the useable signal is decreased even further since it is the nonlinear differential probe transmission signal, $\Delta T * P_{\text{probe}} * \eta$ not the linear probe transmission, which is measured. For the case of the GaAs/AlGaAs samples discussed in this article, the peak differential probe transmission ratio, $\Delta T/T$, is ~0.5%, so typical differential probe transmission signals lie in the pW range.

This pW range signal is accompanied by large background signals which include the transmitted probe power which is unaffected by the pump and the backreflected pump power, which cannot be easily avoided with the NSOM geometry. These background signals dwarf the differential probe transmission signal. Therefore, modulation and lock-in detection is used to differentiate between the differential probe transmission and the unaffected probe and back-reflected pump. Specifically, as mentioned in the previous section, the input pump and probe pulse trains are modulated at 1 and 1.05 MHz, respectively. The effect of pump excitation on probe transmission corresponds to a nonlinear response which mixes the pump and probe signals, introducing a differential probe transmission signal at the 50 kHz difference frequency, which can be measured with lock-in detection. The high frequencies of the pump and probe modulation reduce thermal effects of the tip-sample interaction[13] and, together with the high difference frequency, reduce the effect of laser noise.

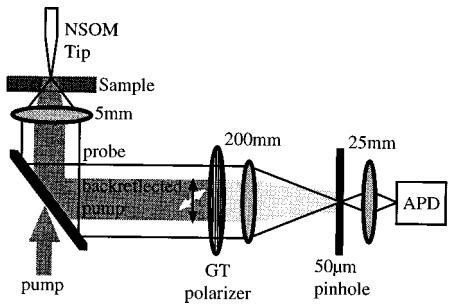

FIG. 2. Detection system, incorporating polarization discrimination and a confocal setup to reduce the back-reflected pump signal. GT: Glan Thomson, APD: avalanche photodiode.

Despite these measures, the unaffected probe and the back-reflected pump can still affect the measurement by increasing the measured shot and laser noise or even saturating the detector. Unfortunately, detection of the unaffected probe signal cannot be avoided, since it cannot be purely optically separated from the desired differential probe signal. Fortunately, this unaffected probe signal is small enough that it does not introduce significant problems, only slightly increasing the noise floor above detector dark noise. However, the back-reflected pump signal is typically many orders of magnitude larger, so that measures need to be taken to reduce this signal as much as possible. In order to avoid the noise and saturation problems associated with detected pump signal, other groups have used two-color setups with spectral filtering[7,9,10] or symmetric arrangements of pump and probe through equal-pulse correlation, sending both pump and probe through the fiber so that both the transmitted pump and unaffected transmitted probe background signals are small.[8] In the experiment described in this article, two measures are taken to reduce the back-reflected pump while avoiding the wavelength limitations of the two-color requirement and the limitations on the measurement flexibility in the equal-pulse setup. These are shown in Fig. 2. First, the pump and probe beams are orthogonally polarized so that a Glan–Thomson polarizer filters out the pump by a factor of typically more than 100, and even as high as 500, while passing most of the probe. Though the polarization of the probe light output from the NSOM tip is not perfectly linear, measurements reveal that the polarization stays quite constant over the pump-probe measurement period. Therefore, no artifacts are introduced into the pump-probe scan by the polarization sensitive

detection. A second method of reducing the back-reflected pump light involves a confocal arrangement consisting of a 50 μm pinhole that spatially filters out the light outside of a 1.25-μm-diam sample area, thereby reducing the back-reflected pump by as much as a factor of 100.

These precautions significantly improve the attainable signal-to-noise ratio of our system, allowing us to measure noise-equivalent powers (NEP) of differential probe transmission signals typically below 1.4 pW (rms), for a 1 s lock-in time constant. For a 10 nW (rms) transmitted probe, this NEP is 1.1 pW (rms), corresponding to a sensitivity in the differential probe transmission ratio, $\Delta T/T$, of $\sim 1 \times 10^{-4}$.

The dominant source of the measured noise in the differential probe transmission signal depends on the total power of the background signals, including both back-reflected pump and unaffected probe. Specifically, for the lowest background signal levels, the measured noise is determined by the dark noise of the detector which, for the case of the avalanche photodiode (APD) module—i.e., APD plus amplifier—used as the photodetector in this system, gives a dark NEP of typically $350\,\mathrm{fW}/\sqrt{\mathrm{Hz}}$. At moderate background signal levels, the measured noise would be dominated by shot noise, which is proportional to the square root of the total detected background signal power. Laser noise grows linearly with the background signal power and only would become significant once one exceeds ~ 1 μW of detected background signal. However, since the background signals in this system range from ~ 5 to ~ 100 nW, the noise in the differential probe transmission signal is largely dominated by shot noise or detector dark noise.

This has effects in the measurable signal to noise ratio. Specifically, if one assumes a small backreflected pump power, then increasing the probe power (for example, by increasing tip aperture diameter) much beyond 1 μW would not improve the signal-to-noise ratio since the laser noise is proportional to the probe power. However, in regions where the differential probe transmission noise is dominated by shot noise or dark noise, i.e., at detected background signal powers below ~ 1 μW, one can improve the signal-to-noise by increasing the probe power.

One artifact of the commercial APD module detection is an electrical mixing of the pump and probe pulses in the module. This introduces a time-delay dependent background signal at the 50 kHz difference frequency at which the differential probe transmission signal is measured. For large back-reflected pump signals, this can be significant enough to warp the pump-probe trace. In all the measurements shown in this article, this mixing effect was sufficiently suppressed by the reduction of the background signals. Nevertheless, new APD designs are being explored which avoid this mixing signal and which reduce the dark noise.

Besides signal-to-noise considerations, time resolution and the limits imposed on it by group velocity dispersion (GVD) is also an important issue. Of highest concern is the GVD of the NSOM fiber, a meter of which can stretch a 100 fs pulse at 800 nm to a chirped 1 ps pulse. Therefore, a GVD precompensation setup was introduced before the fiber coupler in order to add a negative GVD to the pulse, which

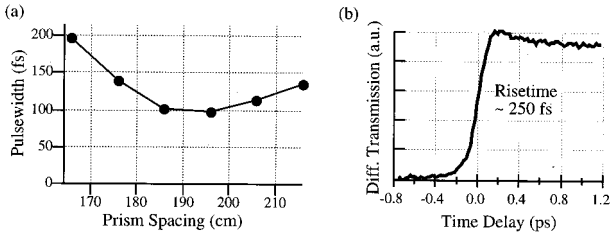

FIG. 3. (a) Measured pulse-width at the output of a 46 cm fiber vs spacing between the prisms of the two-prism GVD precompensation setup, for a ~90 fs input pulse-width, (b) local pump-probe measurement of sample 2, described in a later section, showing a temporal resolution of ~250 fs.

balances the positive GVD of the ~50 cm length of fiber. The GVD precompensator consisted of a standard two-prism setup,[18] in which different spectral components of the pulse travel different distances, introducing a net negative GVD which depends on prism spacing and insertion. Figure 3(a) shows the pulsewidth of the output of a 46 cm open-ended fiber after precompensation, deconvoluted from measured autocorrelation traces, as a function of prism separation, for a 90 fs input pulse. As can be seen, the pulsewidth can be largely recovered with proper GVD optimization. This precompensation should not be affected by the NSOM tip itself, which does not show much effect on GVD.[19] Given this precompensation, we have measured time responses as fast as ~250 fs. This is shown in the pump-probe trace of Fig. 3(b), which was taken on sample 2, described later in this article. The ~250 fs 10%–90% risetime of this signal roughly represents the convolution of the sech^2-shaped pump and probe pulses. This time resolution is partially limited by the ~150 fs pulsewidth of the pump, which was not precompensated for the ~11 cm of glass of the AOM and other optics. It is expected that this time resolution can be further improved by precompensating the pump pulse and also by decreasing the laser output pulsewidth.

One issue of consideration in sending ultrafast pulses through NSOM fibers is the possibility that nonlinear effects in the fiber,[20] such as self phase modulation and stimulated Raman scattering, can warp the spectrum of the measured output pulse. To explore this effect, spectral measurements were made on the outputs of open-ended NSOM fibers, where the ~100 fs input pulses were first precompensated for the NSOM fiber length with the prism setup described in the previous paragraph. These measurements are shown in

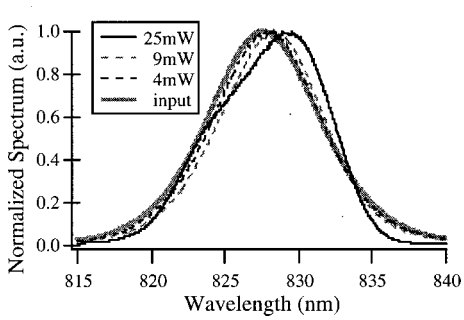

FIG. 4. Spectra of precompensated fiber output pulses for various fiber output powers and fiber input spectrum as a reference.

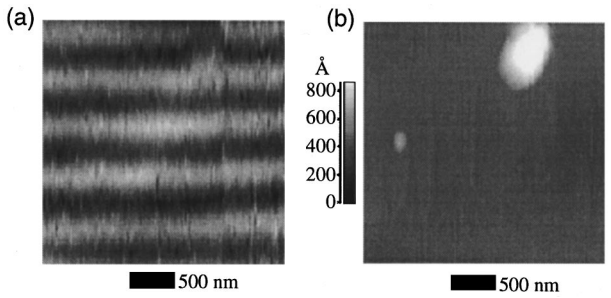

FIG. 5. Two-dimensional scans of pump-probe amplitude at zero time delay (a) and simultaneously measured topographical (b) for sample 1: GaAs/AlGaAs quantum well with 200 nm FIB implanted stripes and 400 nm spaces.

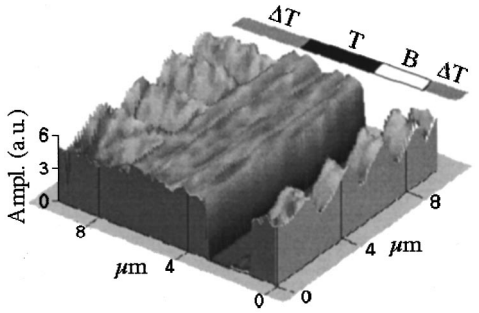

FIG. 6. Two-dimensional scan of sample 2 (GaAs/AlGaAs quantum well with 100 nm FIB implanted stripes and 2 μm spaces) where the measured optical signal is changed during the scan as shown. ΔT: differential probe transmission signal at 40 ps time delay, T: linear probe transmission, B: detector blocked.

Fig. 4. One can see that, for 25 mW output power, the output pulse spectrum is significantly warped with respect to the input pulse spectrum—revealing significant nonlinear effects. However, for output powers below ~4 mW, no significant nonlinear effects were observed. Though these results were measured with open ended fibers, it has been shown that the subwavelength aperture does not have an effect on the spectrum.[21] Therefore, since optical powers within NSOM fibers cannot be much higher than 4 mW due to tip damage, the nonlinear effects are not significant.

Last, a major issue of concern in most NSOM measurements are topographical artifacts[22] in which the topography of the measured surface can alter the optical image, independent of the variation in optical properties. This is of lesser concern in this instrument since the main physics which are explored involves the temporal dependence of the carrier dynamics—i.e., the temporal shape of the pump-probe scan—and how this temporal dependence varies across the sample, issues in which the topographical artifacts are not significant. However, for samples with larger topographical variations, topographical artifacts must be taken into account when interpreting spatial variations in pump-probe amplitudes and in determining spatial resolution.

V. INSTRUMENT PERFORMANCE—FIB SAMPLE RESULTS

In order to prove the capabilities of the system in terms of its performance and its usefulness for measuring interesting physics, samples needed to be measured which had a reasonably predictable lateral variation in carrier dynamics. The samples chosen were undoped 80 Å single quantum well $GaAs/Al_{0.3}Ga_{0.7}As$ samples with a 12 nm top barrier, which were mounted on glass disks and selectively etched to remove the opaque substrates, thus allowing for transmission experiments. Lateral patterning of damage on the nanometer scale was introduced using FIB implantation of Ga ions at 50 keV energies. Such ion implantation is known to reduce the measured nonlinearity and to introduce trap states, leading to fast carrier trapping times.[23,24] These samples then had the advantage of having a flat topographical profile, transition energies suitable to the available 840 nm laser sources, and a designed lateral profile of ion damage which was known to have strong effects on carrier dynamics. Furthermore, the thin top barrier avoided surface trapping effects while the optically active well layer stayed close to the sample surface, thus maintaining good achievable lateral resolution. Two samples were measured, both using the same $GaAs/Al_{0.3}Ga_{0.7}As$ quantum well structures, which varied only in their FIB implantation pattern—200 nm implanted stripes at a $\sim 3\times10^{12}$ ions/cm^2 dose with 400 nm spaces between stripes for sample 1, and 100 nm stripes at a $\sim 8\times10^{11}$ ions/cm^2 dose with 2 μm spaces for sample 2. All measurements were performed at 300 K, exciting at the band edge with a pump fluence of ~4 μJ/cm^2.

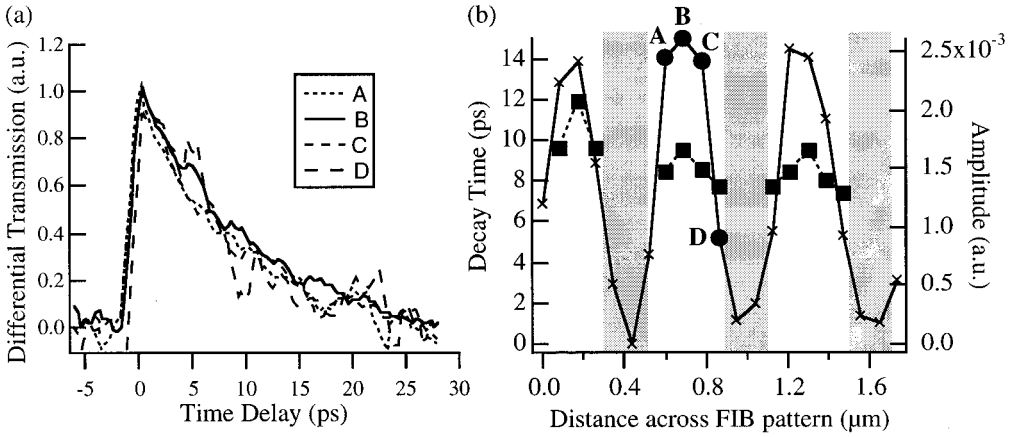

FIG. 7. (a) Normalized pump-probe scans and (b) pump-probe amplitude at zero time delay (×) and decay time from a single-exponential fit (■) vs distance across the sample, for sample 1. The gray region corresponds to the implanted stripe.

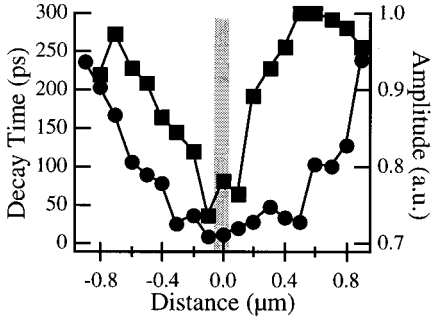

FIG. 8. Fast decay time constant from a double-exponential fit (●) and pump-probe amplitude at zero time delay (■) vs distance across sample 2. The gray region corresponds to the implanted stripe.

Figure 5 shows a two-dimensional (2D) image of the amplitude of the pump-probe signal (at zero time delay) and topography across the area of sample 1. One can clearly distinguish variations in the pump-probe amplitude pattern which follow the 600 nm period of the FIB implantation pattern, where the low signals (dark regions) correspond to smaller nonlinearities expected for higher implantation doses.[23] It should be noted that this pattern is not seen in the topographical plot, proving that the measured optical pattern is not a topographical artifact.[22]

Figure 6 shows a 2D scan of sample 2, in which the NSOM tip was scanned across the surface of the sample while various optical signals were measured—either amplitude of the pump-probe signal (ΔT), linear probe transmission (T), or probe light blocked (B)—as shown. Though the 2 μm periodicity of the implantation profile is clearly visible in the pump-probe amplitude variation, no such correlation is seen in the linear probe transmission profile. This shows that it is the nonlinear response of the sample which is measured, not the linear response.

A series of pump-probe time-domain measurements were taken at various positions across the FIB pattern of Fig. 5. Figure 7(a) shows normalized plots of a few of these scans, while Fig. 7(b) shows the amplitude of these scans and their decay time from a single-exponential fit versus distance across the FIB pattern. The 10%–90% lateral rise in the amplitude plot reveals a lateral resolution as high as ~150 nm. Indeed, this is a conservative estimate of lateral resolution since it assumes a step-like variation in the implantation profile, whereas TRIM[25] simulations suggested that the lateral damage was spread by ~20 nm.

An interesting point in both the normalized pump-probe scans of Fig. 7(a) and the decay time profile of Fig. 7(b) is that the decay time over the region between the stripes is relatively constant at about 8 ps, much smaller than the 100 ps recombination decay times measured in unimplanted areas far away from the implantation-patterned region. This effect cannot be purely due to spatial averaging of the NSOM tip since the amplitude signal shows that variations on this length scale can be spatially resolved. Furthermore, this effect cannot be due to lateral spread of the damage since the large amplitude signal in the unimplanted regions shows that the damage is mainly confined to the 200 nm implanted stripe. Therefore, since the fast decay times cannot be explained by any local characteristic of the material, it must be due to a nonlocal effect of transport. Since drift effects are expected to be insignificant, we conclude that, besides the slow recombination of electron hole pairs, the carrier dynamics in the unimplanted regions of the sample are strongly affected by diffusion, which has also been shown to affect the decay of carriers in other types of semiconductor nanostructures.[8,9,26] Specifically, the initial excited carrier concentration is reduced at the implanted stripes due to fast trapping. The resulting concentration gradient causes carriers in the unimplanted regions to diffuse toward the implanted stripes and get trapped. Therefore, the excited carrier concentrations in the unimplanted regions are quickly depleted by this diffusion process, at a rate which is much faster than the recombination rate and which is relatively independent of the distance across the implantation pattern.

The effect of diffusion on carrier dynamics can also be seen in measurements of sample 2, whose 2 μm spacing allowed us to study carrier dynamics farther away from the FIB stripe. A higher-throughput, ~300 nm aperture size NSOM tip was used here. Figure 8 shows the pump-probe amplitude and fast decay time from a double-exponential fit as a function of distance across the FIB pattern. Indeed, the decay time is roughly constant over a distance of ~800 nm around the implanted stripe—consistent with the results seen on sample 1—and increases to a value equal to the measured recombination time of 250 ps half way between the implanted stripes. The spatial profile of the diffusive component of the decay time roughly follows a quadratic distance dependence.[27] This is plausible since carriers excited close to the edges of the implanted stripe have a shorter distance to diffuse, resulting in enhanced diffusion, whereas diffusion of carriers excited ~1 μm from the stripes is suppressed so that the decay in the carrier population is dominated by recombination. It is clear that the strong variation of the diffusion dynamics on a sub-μm scale could not have been resolved with a far-field system. These results demonstrate that the development of a femtosecond-scale time-resolved NSOM opens up new possibilities for measuring the physics of carrier dynamics in nanometer-scale structures.

ACKNOWLEDGMENTS

The authors would like to acknowledge Dieter Pohl and Renato Zenobi for access to their NSOM tip fabrication facilities; Gunter Steinmeyer for helpful advice on detector considerations; and Andreas Schertel of Micrion, GmbH for FIB implantation. This work was supported by the Swiss National Science Foundation, program NFP 36.

[1] J. Shah, *Ultrafast Spectroscopy of Semiconductors and Semiconductor Nanostructures* (Springer, Berlin, 1996).
[2] M. Chergui, *Femtochemistry* (World Scientific, Singapore, 1996).
[3] E. Kapon, in *Optical Spectroscopy of Low-Dimensional Semiconductors*, edited by G. Abstreiter *et al.* (Kluwer Academic, Amsterdam, 1997).
[4] M. A. Paesler and P. J. Moyer, *Near-Field Optics: Theory, Instrumentation, and Applications* (Wiley, New York, 1996).
[5] D. W. Pohl, W. Denk, and M. Lanz, Appl. Phys. Lett. **44**, 651 (1984).
[6] E. Betzig and J. K. Trautman, Science **257**, 189 (1992).
[7] J. B. Stark, U. Mohideen, and R. E. Slusher, Tech. Dig. Ser. Conf. Ed. **16**, 82 (1995).

[8] S. Smith, N. C. R. Holme, B. Orr, R. Kopelman, and T. Norris, Ultramicroscopy **71**, 213 (1998).
[9] J. Levy, V. Nikitin, J. M. Kikkawa, A. Cohen, N. Samarth, R. Garcia, and D. D. Awschalom, Phys. Rev. Lett. **76**, 1948 (1996).
[10] A. Vertikov, M. Kuball, A. V. Nurmikko, and H. J. Maris, Appl. Phys. Lett. **69**, 2465 (1996).
[11] S. Jiang, H. Ohsawa, K. Yamada, T. Pangaribuan, M. Ohtsu, K. Imai, and A. Ikai, Jpn. J. Appl. Phys., Part 1 **31**, 2282 (1992).
[12] C. L. Tang and D. J. Erskine, Phys. Rev. Lett. **51**, 844 (1983).
[13] A. H. Rosa, B. I. Yakobson, and H. D. Hallen, Appl. Phys. Lett. **67**, 2597 (1995).
[14] M. Stähelin, M. A. Bopp, G. Tarrach, A. J. Meixner, and I. Zschokke-Gränacher, Appl. Phys. Lett. **68**, 2603 (1996).
[15] E. Betzig, P. L. Finn, and J. S. Weiner, Appl. Phys. Lett. **60**, 2484 (1992).
[16] K. Karrai and R. D. Grober, Appl. Phys. Lett. **66**, 1842 (1995).
[17] H. A. Bethe, Phys. Rev. **66**, 163 (1944).
[18] F. J. Duarte and J. A. Piper, Opt. Commun. **43**, 303 (1982).
[19] S. Smith, B. G. Orr, R. Kopelman, and T. Norris, Ultramicroscopy **57**, 173 (1995).
[20] G. P. Agrawal, *Nonlinear Fiber Optics* (Academic, New York, 1989).
[21] A. Lewis, U. Ben-Ami, N. Kuck, G. Fish, D. Diamant, L. Lubovsky, K. Lieberman, S. Katz, A. Saar, and M. Roth, Scanning **17**, 3 (1995).
[22] B. Hecht, H. Bielefeldt, Y. Inouye, and D. W. Pohl, J. Appl. Phys. **81**, 2492 (1997).
[23] M. J. Lederer, B. Luther-Davies, H. H. Tan, C. Jagadish, M. Haiml, U. Siegner, and U. Keller (unpublished).
[24] M. Lambsdorff, J. Kuhl, J. Rosenzweig, A. Axmann, and J. Schneider, Appl. Phys. Lett. **58**, 1881 (1991).
[25] J. F. Ziegler, J. P. Biersack, and U. Littmark, *The Stopping and Range of Ions in Solids* (Pergamon, New York, 1989), Vol. 1.
[26] A. Richter, G. Brehme, M. Süptitz, C. Lienau, T. Elsässer, M. Ramsteiner, R. Nötzel, and K. H. Ploog, Phys. Rev. Lett. **79**, 2145 (1997).
[27] B. A. Nechay, U. Siegner, F. Morier-Genoud, A. Schertel, and U. Keller, Appl. Phys. Lett. **74**, 61 (1999).